Supplementary Materials for

Gene Regulatory Network topology governs resistance and treatment escape in glioma stem-like cells

James H. Park[1], Parvinder Hothi[2], Adrian Lopez Garcia de Lomana[3], Min Pan[1], Rachel Calder[1], Serdar Turkarslan[1], Wei-Ju Wu[1], Hwahyung Lee[2], Anoop P. Patel[4,5], Charles Cobbs[2], Sui Huang[1], Nitin S. Baliga[1,6,*]

1. Institute for Systems Biology, Seattle, WA.
2. Ivy Center for Advanced Brain Tumor Treatment, Swedish Neuroscience Institute, Seattle, WA.
3. Center for Systems Biology, University of Iceland, Reykjavik, Iceland.
4. Department of Neurosurgery, Preston Robert Tisch Brain Tumor Center, Duke University, Durham, NC.
5. Center for Advanced Genomic Technologies, Duke University, Durham, NC
6. Departments of Microbiology, Biology, and Molecular Engineering Sciences, University of Washington, Seattle, WA.

Corresponding author email: nitin.baliga@isbscience.org

This PDF file includes:

Supplementary Text
Figs. S1 to S17

Other Supplementary Materials for this manuscript include the following:

Tables S1 to S16

Supplementary Text

Selection and proliferation of mesenchymal GSCs does not account for changes in PD-GSC population structure

Given the mounting evidence supporting the ability of GSCs to undergo cell state transitions in response to drug treatment, exemplified in PMT, it was likely that the shift in the proportion of molecular subtypes observed in SN520 was due to such a transition. However, the shift in molecular subtype could have been the result of the selection of a pre-existing subpopulation of MES cells. To confirm whether changes in population structure occurring in PD-GSCs were due to non-genetic changes in cell state or drug-induced selection, we performed both theoretical calculations and DNA quantification to determine the feasibility of a selection process driving the observed changes in SN520 population structure. Using the population structure and number of cells collected at each time point, we considered three scenarios for our theoretical calculations: 1) only pre-existing MES cells survived treatment with negligible proliferation, 2) only pre-existing MES cells survive and proliferate, and 3) assuming selection was the driving force, what cell doubling time (t_d) would be required to produce cell counts observed.

We analyzed multiple scenarios under which a change in population structure could occur: *i)* Selection of MES PD-GSCs, *ii)* selection and proliferation of MES PD-GSCs only, and *iii)* concurrent proliferation of MES PD-GSCs and death of all non-MES PD-GSCs. In all scenarios, cell counts and estimated t_d for SN520 were used (Supplementary Figure S7).

In scenario *i)*, the simplest case – we assumed that the initial amount of MES cells at D0 (24,657 cells) remained consistent through the 4-day experiment. As we estimated 537,500 total viable cells (based on calculated cell concentrations and volumes collected) by the end of the 4-day pitavastatin treatment, the proportion of MES PD-GSCs would only account for 4.6% of the total PD-GSC population, which differs tremendously from the 94% proportion present in the surviving cells (505,421 MES PD-GSCs). Alternatively, had a majority of the non-MES PD-GSCs died during treatment, it is theoretically possible that the MES subtype could make up 94% of the surviving cells, if not more. The theoretical final cell counts, however, would not match with experimental results.

In scenario *ii)* we analyzed an extension of scenario *i)* alternative in that it was assumed that all non-MES PD-GSCs were eliminated by the end of the 4-day treatment and that only MES PD-

GSCs grew during this time. To estimate final cell amounts by D4, we assumed exponential growth, characterized by the following:

$$x_f = x_i * 2^n \quad \text{Eqn. 1}$$

Where x_f is final number of PD-GSCs, $x_i$is the initial number of PD-GSCs, and n is the number of doublings that occurred. Here the number of doublings is equivalent to

$$n = \frac{\Delta t}{t_d} \quad \text{Eqn. 2}$$

Where Δt is the duration of the experiment and t_d is the doubling time. In this case, SN520 had a doubling time of ~85hrs (Supplementary Figure S7). Based on Eqns. 1 and 2, the total number of MES PD-GSCs totaled 51,421 cells, which also falls short of the 537,500 cells (505,421 MES PD-GSCs) at D4.

In scenario *iii)* we determined what t_d would be required of the MES cells to match experimental observations. Based on the initial and final number of MES PD-GSCs, 24,658 and 51,421 cells, respectively, and a 3.94-day duration time, we found that t_d of 21.9hr would be required for the initial number of MES cells to match experimentally measured cell counts and subtype proportions at D4. This suggests that MES cells experienced an approximate 4-fold decrease in t_d relative to the rest of the PD-GSC population, which is highly unlikely. It is important to note that these theoretical calculations assumed ideal or maximal growth rates for the MES cells. In other words, despite calculations, which favored MES growth, some other factor or process most likely contributed to the increase in proportions of MES cells. These results, taken together with the low number of PD-GSCs in the G2/M phase, based on cell cycle annotation and DNA quantification, strongly point towards pitavastatin treatment inducing a MES transition in SN520.

Differential Expression Gene and Clustering Enrichment Analysis

DEG and enrichment analysis revealed several insights into the cellular response and sequence of responses for each PD-GSC. As SN520 expressed a clear coordinated response during treatment, we provide additional details on the results from the DEG and enrichment analyses.

SN520 Clustering & Enrichment. Vehicle control cells of SN520 from all time points were evenly distributed across eight Leiden clusters (cl_{520}-0, cl_{520}-1, cl_{520}-3, cl_{520}-5, cl_{520}-8, cl_{520}-10, and cl_{520}-11), a majority of which were enriched for genes of oxidative phosphorylation (OXPHOS) and growth-related hallmark pathways like E2F targets and G2M checkpoint (Figure 3E, table S2). Together these findings suggested that, in the absence of drug treatment, SN520 cells proliferated using OXPHOS as a mode of energy production *(96, 97)*. By contrast, six clusters (cl_{520}-2, cl_{520}-4, cl_{520}-6, cl_{520}-7, cl_{520}-12, and cl_{520}-13) were predominantly enriched with cells from a single pitavastatin-treatment time point. In fact, Leiden clusters could be organized longitudinally based on the relative proportions of drug-treated cells from each day to recreate the likely sequence of events triggered by pitavastatin *(43)* (Figure 3C). For instance, temporal ordering of D2 and D3 pitavastatin-treated cell clusters (cl_{520}-2 → cl_{520}-9 → cl_{520}-4 → cl_{520}-7) revealed sequential differential regulation of cholesterol homeostasis, fatty acid metabolism, MTORC1 signaling, a regulator of lipid formation *(98)*, and cholesterol biosynthesis and maintenance. This sequential differential regulation of functions across D2 and D3 cells was consistent with the mechanism of action of pitavastatin (i.e., inhibition of cholesterol biosynthesis). In addition, enrichment of apoptosis (cl_{520}-4, cl_{520}-6, and cl_{520}-7) and TNFα signaling via NFκB (cl_{520}-6 and cl_{520}-7), with progressively higher proportions of D4 pitavastatin-treated cells suggested a mechanism of killing by pitavastatin. Specifically, the findings showed that on D4, pitavastatin treatment had induced TNF-α signaling, which activated apoptosis within a subpopulation of SN520 GSCs and was consistent with both annexin V cytometry results (Supplementary Figure S2) and timing of maximal cell death rate (Figure 1B). Further, the high proportion of D4 pitavastatin-treated cells in cl_{520}-6 and cl_{520}-7 indicated that the cytotoxic effects resulted in the upregulation of cellular stress responses including unfolded protein response, protein secretion, and p53 pathway.

As described in the main text, cl_{520}-6, cl_{520}-7, and cl_{520}-13, which were cell clusters enriched with D4 pitavastatin-treated cells, were enriched for both apoptosis- and EMT-associated genes and contained cells from time points that aligned with the timing of the MES transition (Figure 2C, D). These findings were consistent with previous studies that reported TGF-β can simultaneously induce apoptosis and EMT during tumor formation and progression. Cell fate correlated with cell-cycle phase, with tumor cells in G2/M phase undergoing apoptosis and those in G1/S phase undergoing EMT *(37, 38)*. As cells in cl_{520}-6, cl_{520}-7, and cl_{520}-13 were in G1/S phase, explaining how surviving SN520 PD-GSCs might have escaped apoptosis – by transitioning into the MES subtype (Supplementary Figure S8). Finally, a majority of Leiden clusters did upregulate genes associated with autophagy (table S2), which aligns with previously reported mechanisms of

pitavastatin in glioma cells *(30)* and suggests that autophagy played a role in the response of SN520.

TF-TF network modeling and ODE simulation motivation

As characterization of drug response at single-cell resolution strongly supported the notion that the PD-GSCs underwent drug-induced transitions, we sought to understand how transcriptional regulatory mechanisms could govern the phenotypic heterogeneity observed within and across the two PD-GSC populations. Thus, we investigated the dynamical behavior of the underlying transcriptional regulatory networks from which multiple steady states, i.e., phenotypic states, emerge. The TFs comprising each core network were all associated with response-relevant processes (table S13) *(26, 36, 44, 99–149)*. Using the core TF-TF networks (Figure 4E, F), we applied a previously developed algorithm known as random circuit perturbation (RACIPE) *(63, 64)*, originally designed to model EMT circuits in cell development and other cancers *(65–67)*. Briefly, RACIPE generates an ensemble of ordinary differential equation (ODE) models based on associated chemical rate equations with distinct, random kinetic parameter sets. Because distinct, random kinetic parameters sets are used, this avoids the issue of parameter identification for kinetic-based ODE models. From the ensemble of models, we analyzed the resulting distribution of steady states and identified robust phenotypes supported by the core TF network. Previous applications have demonstrated that this ensemble modeling/simulation approach was able to recapitulate established cell states in the context of EMT-associated metastasis, B-cell lymphopoiesis, and small cell lung cancer *(62, 63, 150, 151)*.

TF-TF network validation for SN520 and SN503

To test the predictive capabilities of the TF-TF network topologies, we evaluated how similar or dissimilar the simulated states were to experimental data when each network was initialized using untreated (D0) data for each PD-GSC, respectively. Hierarchical clustering of the simulated steady states for both SN520 and SN503 resulted in four main clusters, i.e., “robust” steady states for each PD-GSC (Fig 6C, E – dendrogram of simulated states). We then determined pairwise cosine similarity values derived from pairwise comparisons of *i)* PD-GSCs to one another within each hierarchical cluster and *ii)* simulated states to PD-GSCs within hierarchical clusters. Of the latter comparisons, when clusters of simulated states were similar to experimental clusters, the distributions of cosine similarity values were significantly higher than distributions based on comparisons in which TF gene expression was randomly permuted (Supplementary Figure S12).

To assess the statistical significance of the network topologies, we also performed simulations in which nodes and edges were randomly assigned such that the number of nodes and connections within each permuted network is identical to that of the original corresponding network. Using the same untreated (D0) TF expression values as initial conditions, we performed RACIPE simulations using 1,000 permutated networks, where each permuted network was used to run 1,000 randomly selected parameter sets with a randomly selected untreated (D0) TF expression profile. The resulting 1e6 simulated states for each PD-GSC were then compared to the TF expression profiles of untreated and pitavastatin-treated cells to create a null distribution of cosine similarity values. Using this null distribution as a basis of comparison, we found that cosine similarity values derived from the original TF-TF network topologies were statistically significant (SN520 p-value < 1e-16, SN503 p-value < 1e-16, Supplementary Figure S12).

Assessment of pitavastatin as an HDAC-inhibitor

Prior reports have suggested that statins affect gene expression epigenetically through the inhibition of histone deactylases (HDACs). Lin et al. *(152)* and Mohammadzadeh et al. *(153)* reported potential role of statins in histone modification. However, pitavastatin was not explicitly included in their analyses. In contrast, Bridgeman et al. reported contrasting findings, stating that statins did not directly inhibit the activity of major epigenetic-modifying enzymes including HDAC *(154)*.

To clarify these the contradictory findings, we investigated whether the effects of pitavastatin were mediated through HDACi. Specifically, we determined if signatures of HDAC inhibition (HDACi) were reflected in SN520 and SN503. We leveraged a recent study by Rampazzo et al. *(155)* that had reported differentially expressed genes (DEGs) in primary GSC lines treated with HDACi. Out of the 1,112 HDACi-induced DEGs, only a small number of genes were also upregulated by pitavastatin treatment in SN520 (responder) on D2 – D3 (28 and 44 genes, respectively, table S15). In SN503 (non-responder), there was no significant overlap between HDACi-induced and pitavastatin-upregulated DEGs (table S15). Moreover, phenotypic effects of pitavastatin on SN520 and SN503 were also distinct from those HDACi-induced effects previously reported. Specifically, Rampazzo et al. reported that HDACi decreased WNT signaling, which resulted in repression of stem-like phenotype of GSCs and induced transition of GSCs to a neuronal state. In stark contrast, we observed that pitavastatin treatment led to increased WNT signaling, and drove PMT in SN520 (Figure 4). In addition, pitavastatin treatment did not cause changes in stem cell-like phenotypes in either SN520 or SN503 as expression of at least one stem cell surface

194 protein marker, CD133 or CD44 was maintained in both PD-GSCs throughout treatment (Figures
195 2E, F). Together, these findings cast significant doubt that gene expression changes induced by
196 pitavastatin in SN520 and SN503 were mediated by HDACi.

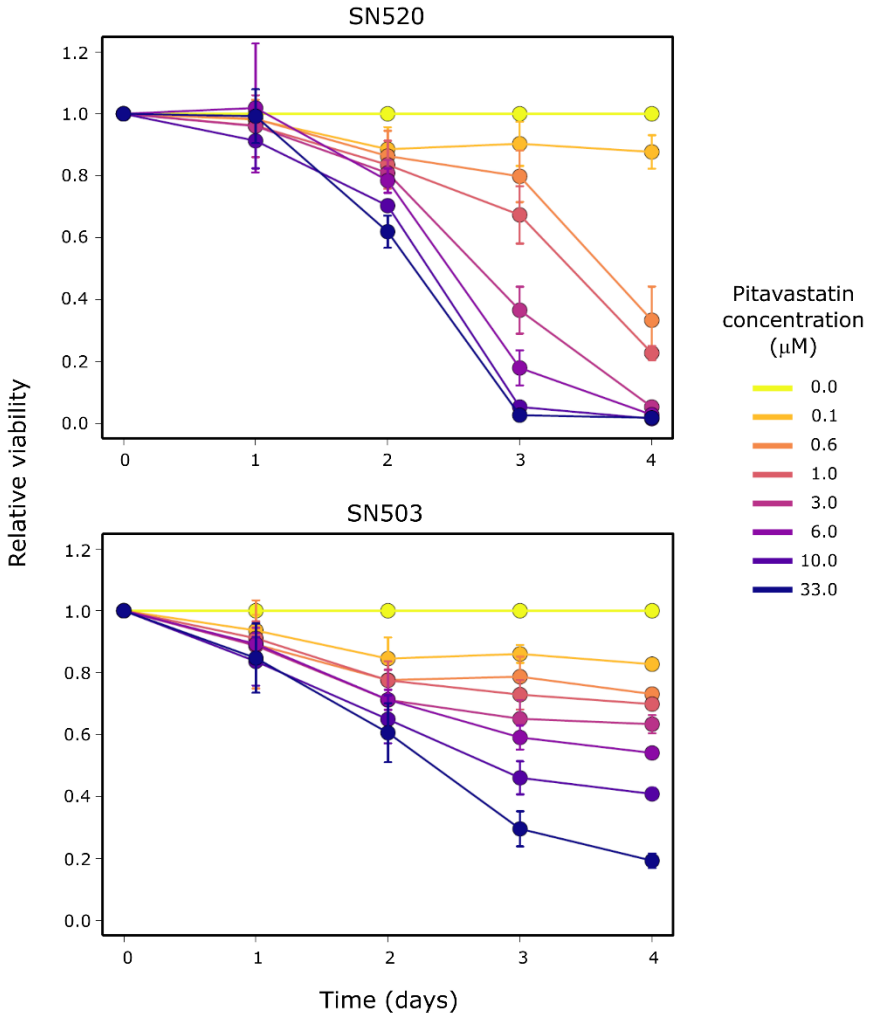

Fig. S1. Pitavastatin-induced kill kinetics in SN520 and SN503. Plots of mean cell viability during pitavastatin treatment for SN520 (top) and SN503 (bottom). Each series of relative viability values corresponds to a different pitavastatin concentration. Relative viability was calculated with respect to the untreated (vehicle-normalized, pitavastatin = 0.0μM) condition. Plotted values are mean viability values (N = 3) and error bars represent ±2x standard deviation.

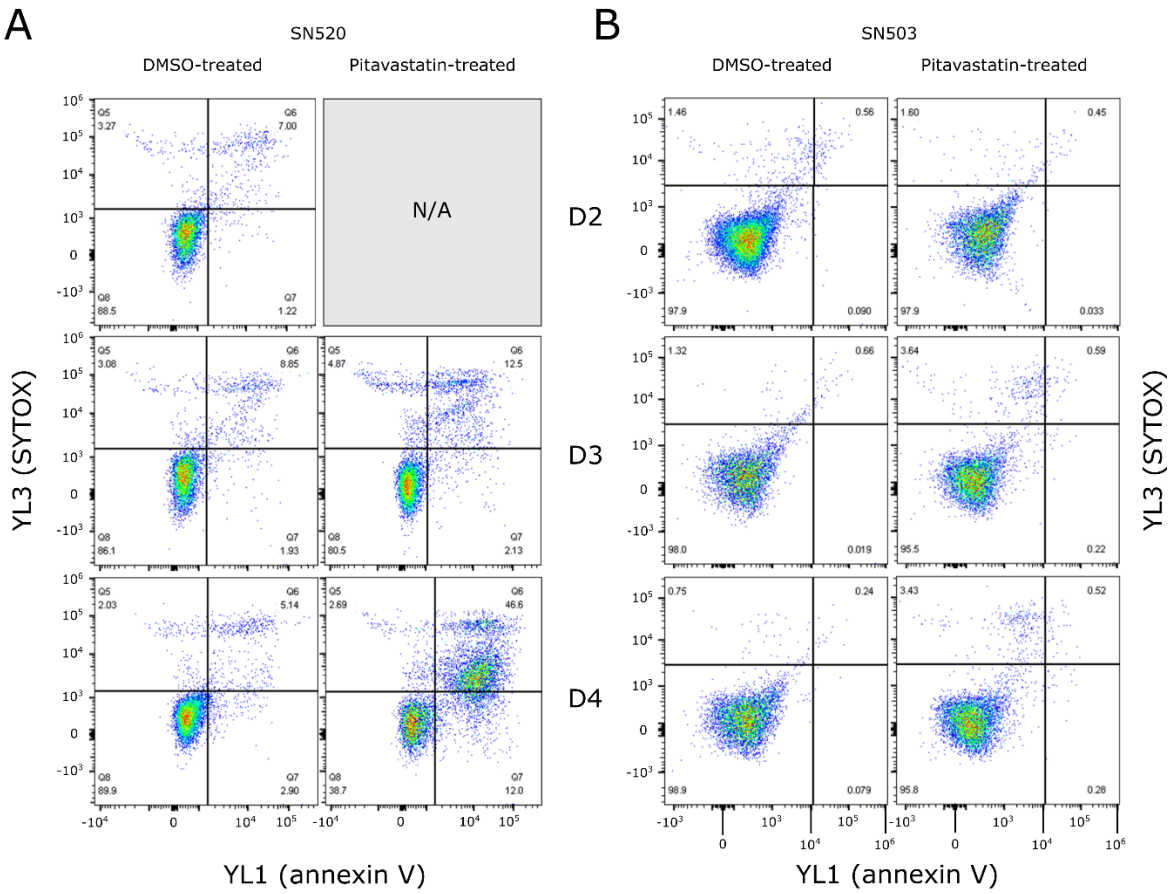

205

206 **Fig. S2. Flow cytometry analysis of apoptosis and cell death.** Dot plots of cells assessing cell
207 death (SYTOX) and apoptotic markers (annexin V) for **(A)** SN520 and **(B)** SN503. Gating was
208 based on an unstained control and heat-inactivated/live cell (50:50) mixed control sample for each
209 PD-GSC. Heat inactivation consisted of incubating cells in 60°C water bath for 15 minutes, with
210 a small sample being inspected post incubation under microscope to ensure that inactivated cells
211 were not completely lysed. Due to sample-limitations in D2 pitavastatin treated samples, flow
212 cytometry assessment of cell-death and apoptosis was not performed (N/A plot).

213

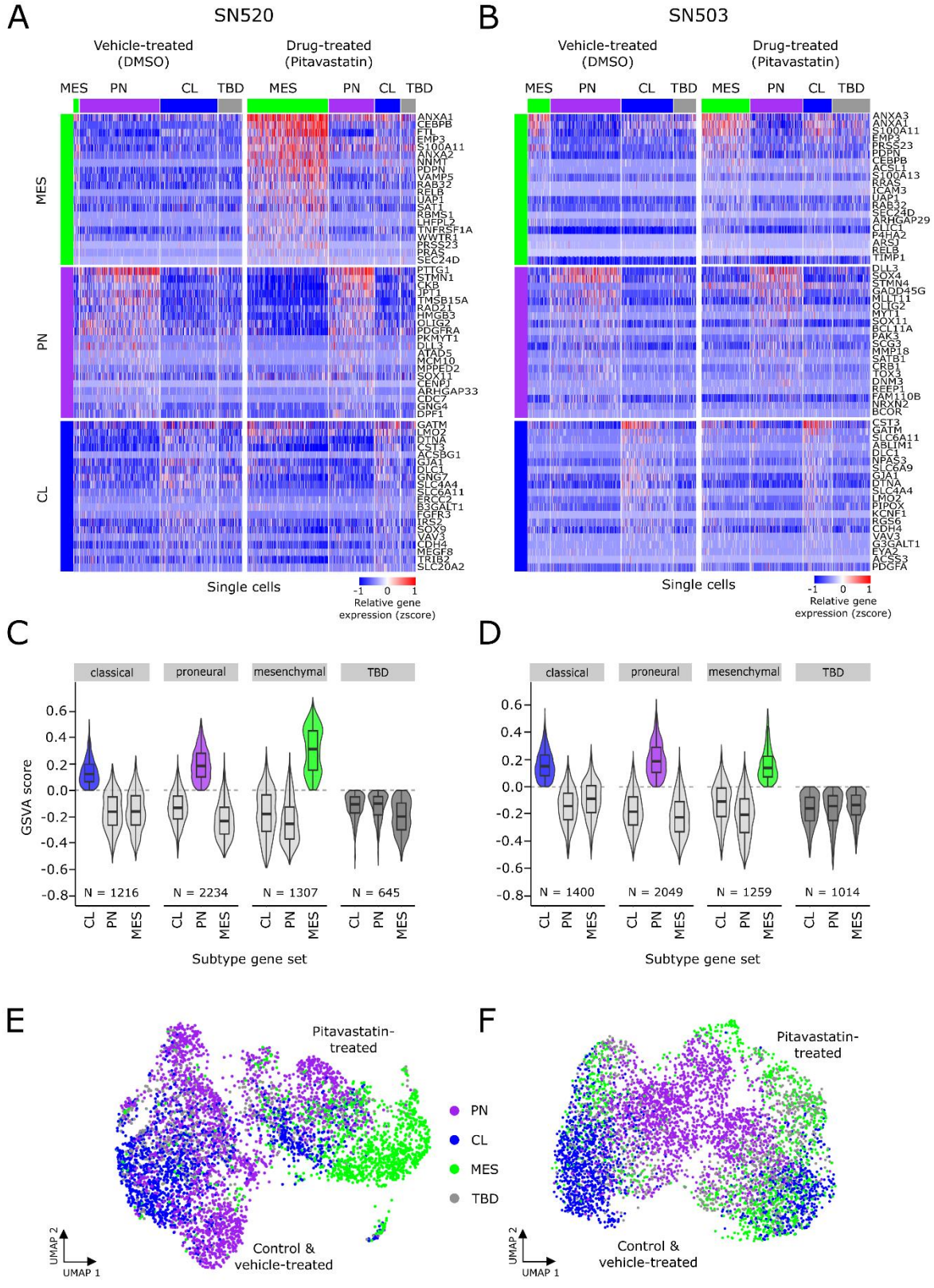
A
SN520
Vehicle-treated (DMSO)
Drug-treated (Pitavastatin)
MES PN CL TBD MES PN CL TBD
MES
PN
CL
ANXA1 CEBPB FTL EMP3 S100A11 ANXA2 NNMT PDPN VAMP5 RAB32 RELB UAP1 SAT1 RBMS1 LHFPL2 TNFRSF1A WWTR1 PRSS23 PRAS SEC24D
PTTG1 STMN1 CKB JPT1 TMSB15A RAD21 HMGB3 OLIG2 PDGFRA PKMYT1 DLL3 ATAD5 MCM10 MPPED2 SOX11 CENPT ARHGAP33 CDC7 GNG4 DPF1
GATM LMO2 DTNA CST3 ACSBG1 GJA1 DLC1 GNG7 SLC4A4 SLC6A11 ERCC2 B3GALT1 FGFR3 IRS2 SOX9 VAV3 CDH4 MEGF8 TRIB2 SLC20A2
Single cells
-1 0 1
Relative gene expression (zscore)
B
SN503
Vehicle-treated (DMSO)
Drug-treated (Pitavastatin)
MES PN CL TBD MES PN CL TBD
ANXA3 ANXA1 S100A11 EMP3 PRSS23 PDPN CEBPB ACSL1 S100A13 RRAS ICAM3 UAP1 RAB32 SEC24D ARHGAP29 CLIC1 P4HA2 ARSJ RELB TIMP1
DLL3 SOX4 STMN4 GADD45G MLLT11 OLIG2 MYT1 SOX11 BCL11A PAK3 SCG3 MMP18 SATB1 CRB1 TOX3 DNM3 REEP1 FAM110B NRXN2 BCOR
CST3 GATM SLC6A11 ABLIM1 DLC1 NPAS3 SLC6A9 GJA1 DTNA SLC4A4 LMO2 PIPOX KCNF1 RGS6 CDH4 VAV3 G3GALT1 EYA2 ACSS3 PDGFA
Single cells
-1 0 1
Relative gene expression (zscore)
C
classical proneural mesenchymal TBD
GSVA score
0.6 0.4 0.2 0.0 -0.2 -0.4 -0.6 -0.8
N = 1216 N = 2234 N = 1307 N = 645
CL PN MES CL PN MES CL PN MES CL PN MES
Subtype gene set
D
classical proneural mesenchymal TBD
0.6 0.4 0.2 0.0 -0.2 -0.4 -0.6 -0.8
N = 1400 N = 2049 N = 1259 N = 1014
CL PN MES CL PN MES CL PN MES CL PN MES
Subtype gene set
E
Pitavastatin-treated
Control & vehicle-treated
UMAP 2
UMAP 1
PN
CL
MES
TBD
F
Pitavastatin-treated
Control & vehicle-treated
UMAP 2
UMAP 1

Fig. S3. Defining GBM molecular subtypes via gene expression. Heatmaps of subset of 20 genes used to define GBM molecular subtypes for **(A)** SN520 and **(B)** SN503 cells. Violin/boxplots of GSVA enrichment scores (ES) for CL, PN, and MES molecular subtypes determined for cells. Clusters of violin/boxplots correspond to molecular subtype scores for cells categorized to each subtype for **(C)** SN520 and **(D)** SN503. Numbers of single cells belonging to each subtype are listed underneath violin/boxplots. Those cells having a negative ES for all three subtypes remained undefined (TBD - grey). UMAP plots show PD-GSCs annotated according to enriched molecular subtype for **(E)** SN520 and **(F)** SN503.

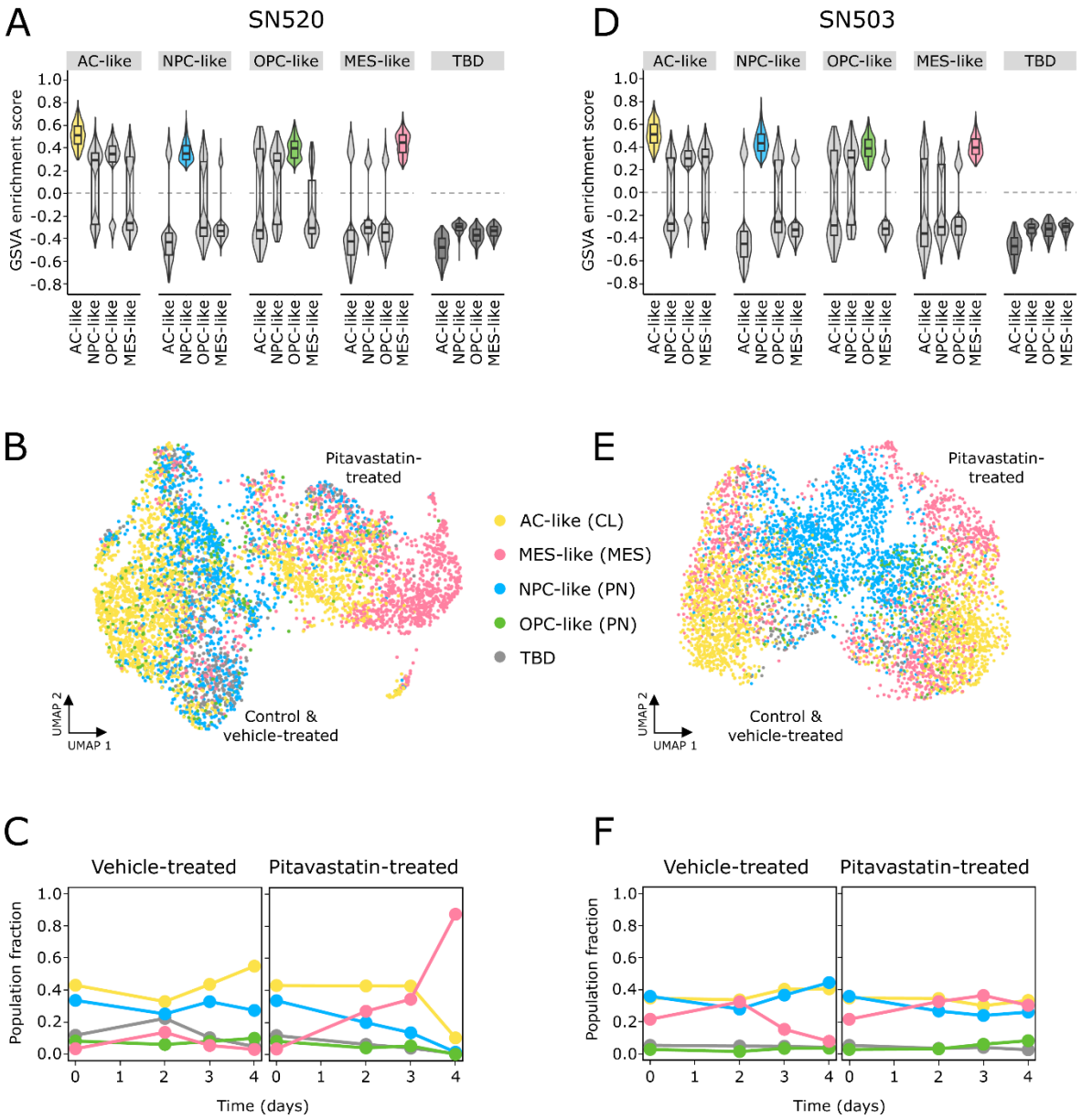

Fig. S4. Cell state annotation of SN520 and SN503. (A) Violin/boxplots of GSVA enrichment scores (ES) for AC-like, NPC-like, OPC-like, and MES-like cell states (*9*) for SN520 cells. **(B)** UMAP plots of PD-GSCs annotated according to enriched cell states. **(C)** Proportions of cell states across treatment and time points for SN520. **(D-F)** Corresponding plots for SN503. Color annotation for (E, F) are identical to that in (B, C).

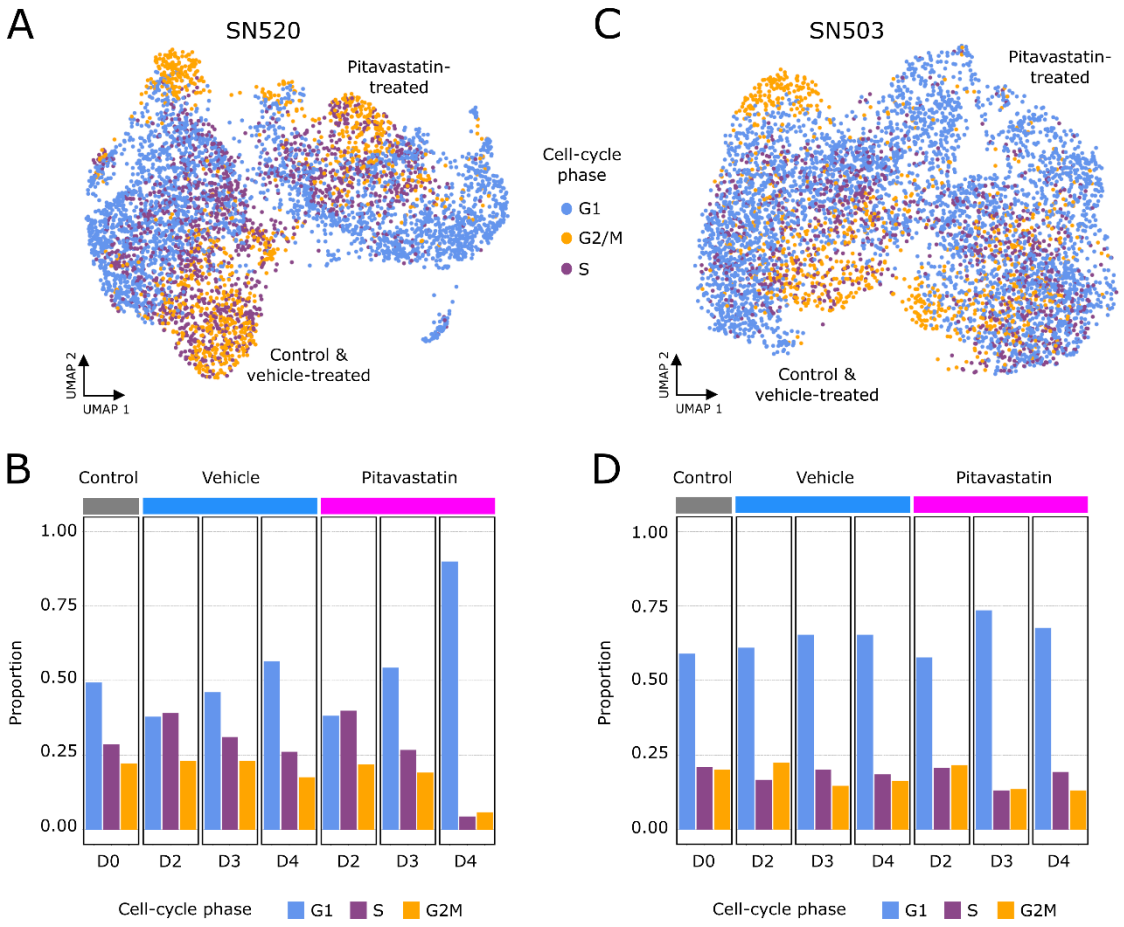

Fig. S5. Cell cycle phase breakdown of SN520 and SN503. (A) UMAP plot of SN520, similar to Figure 2A, annotated for cell cycle phase for each cell. **(B)** Proportions of cells in each cell cycle phase within each treatment condition for SN520. **(C)** UMAP plot of SN503 annotated for cell cycle phase for each cell. **(D)** Proportions of cells in each cell cycle phase within each treatment condition for SN503.

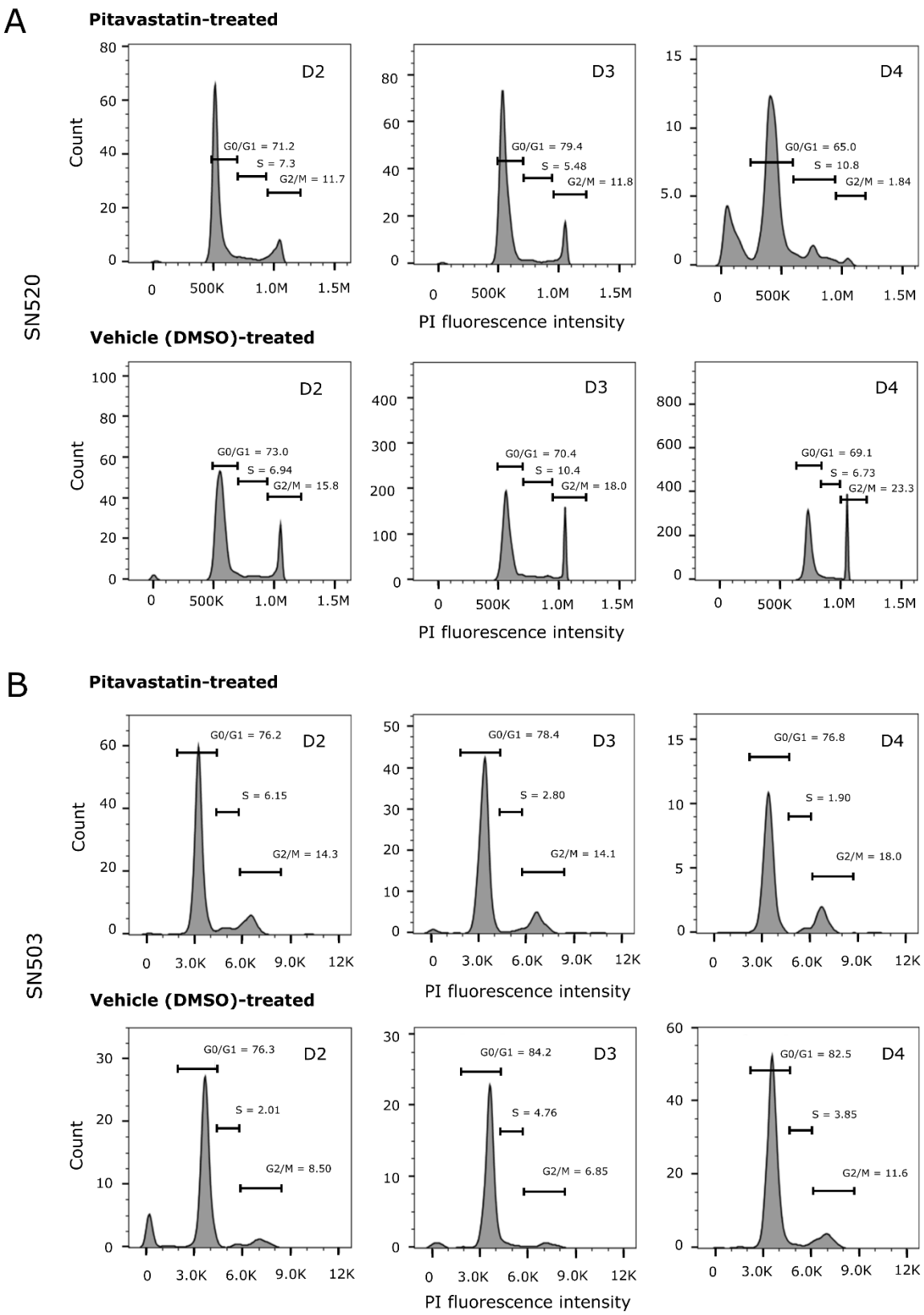
A
Pitavastatin-treated
SN520
D2
D3
D4
Count
G0/G1 = 71.2
S = 7.3
G2/M = 11.7
G0/G1 = 79.4
S = 5.48
G2/M = 11.8
G0/G1 = 65.0
S = 10.8
G2/M = 1.84
PI fluorescence intensity
Vehicle (DMSO)-treated
G0/G1 = 73.0
S = 6.94
G2/M = 15.8
G0/G1 = 70.4
S = 10.4
G2/M = 18.0
G0/G1 = 69.1
S = 6.73
G2/M = 23.3
B
Pitavastatin-treated
SN503
G0/G1 = 76.2
S = 6.15
G2/M = 14.3
G0/G1 = 78.4
S = 2.80
G2/M = 14.1
G0/G1 = 76.8
S = 1.90
G2/M = 18.0
Vehicle (DMSO)-treated
G0/G1 = 76.3
S = 2.01
G2/M = 8.50
G0/G1 = 84.2
S = 4.76
G2/M = 6.85
G0/G1 = 82.5
S = 3.85
G2/M = 11.6

Fig. S6. DNA quantification throughout treatments. Density plots of fluorescent signals generated from cells stained with propidium iodide (PI) throughout pitavastatin- (top) and vehicle-treatment (bottom) for **(A)** SN520 and **(B)** SN503. Portions of the density plots representative of specific cell cycle phases have been labeled, along with percentages of cells within each phase.

A

PD-GSC ID	Incoulation density (cells)	Passage/harvest density (cells)	Growth duration (days)	Substrate	Estimted t_d (hrs)
SN520	4.36E+05	7.56E+06	14	T75 flask	81.62
SN520	4.36E+05	7.48E+06	14	T75 flask	81.93
SN520	4.36E+05	5.94E+06	14	T75 flask	89.17
SN503	5.68E+05	5.58E+06	13	T75 flask	94.65
SN503	5.68E+05	4.22E+06	13	T75 flask	107.79
SN503	5.68E+05	4.40E+06	13	T75 flask	105.59

	mean t_d (hrs)
SN520	84.24
SN503	102.68

	Percent MES	Total viable cells (D4)	Total MES cells (D4)
SN520	94.03%	537,500	505,421

B

Scenario *i*

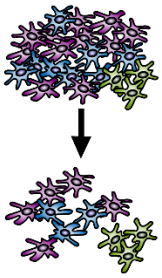

Time (day)	Total cell count	MES fraction	MES cell count
0	1.200E+06	0.021	2.466E+04

constant number of MES cells

4	5.375E+05	0.046	2.466E+04

Scenario *ii*

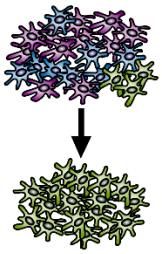

Time (day)	Total cell count	MES fraction	MES cell count
0	1.200E+06	0.021	2.466E+04

$x_f = x_i * 2^n$
$n = \Delta t / t_d$
$t_d = 84.24$ *hrs (SN520)*

4	5.407E+04	1.000	5.40E+04

Scenario *iii*

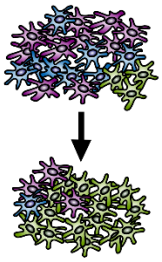

Time (day)	Total cell count	MES fraction	MES cell count
0	1.200E+06	0.021	2.466E+04
4	5.375E+05	0.940	5.054E+05

required $t_d = \Delta t / (log2(x_f/x_i))$
required $t_d = 21$ *hrs*
original $t_d = 21$ *hrs*

Proneural Classical Mesenchymal

Fig. S7. Theoretical calculations corroborate PMT rather than selection. (A) Summary of cell counts (top table) used to determine doubling times (t_d) for SN520 and SN503 (middle table). Summary of total cell counts and estimated D4 MES cell counts for SN520 at D4 are listed in bottom table. **(B)** Calculations supporting three scenarios that potentially explain the increase in the proportion of MES cells within SN520. Scenario *i*) assumes a selection of pre-existing MES PD-GSCs. Scenario *ii*) assumes exponential growth of MES cells only with a t_d based on (A). Finally, scenario *iii)* assumes exponential growth of MES cells, but determines a t_d that would enable MES growth to match final SN520 cell counts on the fourth day of pitavastatin treatment. The corresponding t_d required to achieve a final MES cell count is listed.

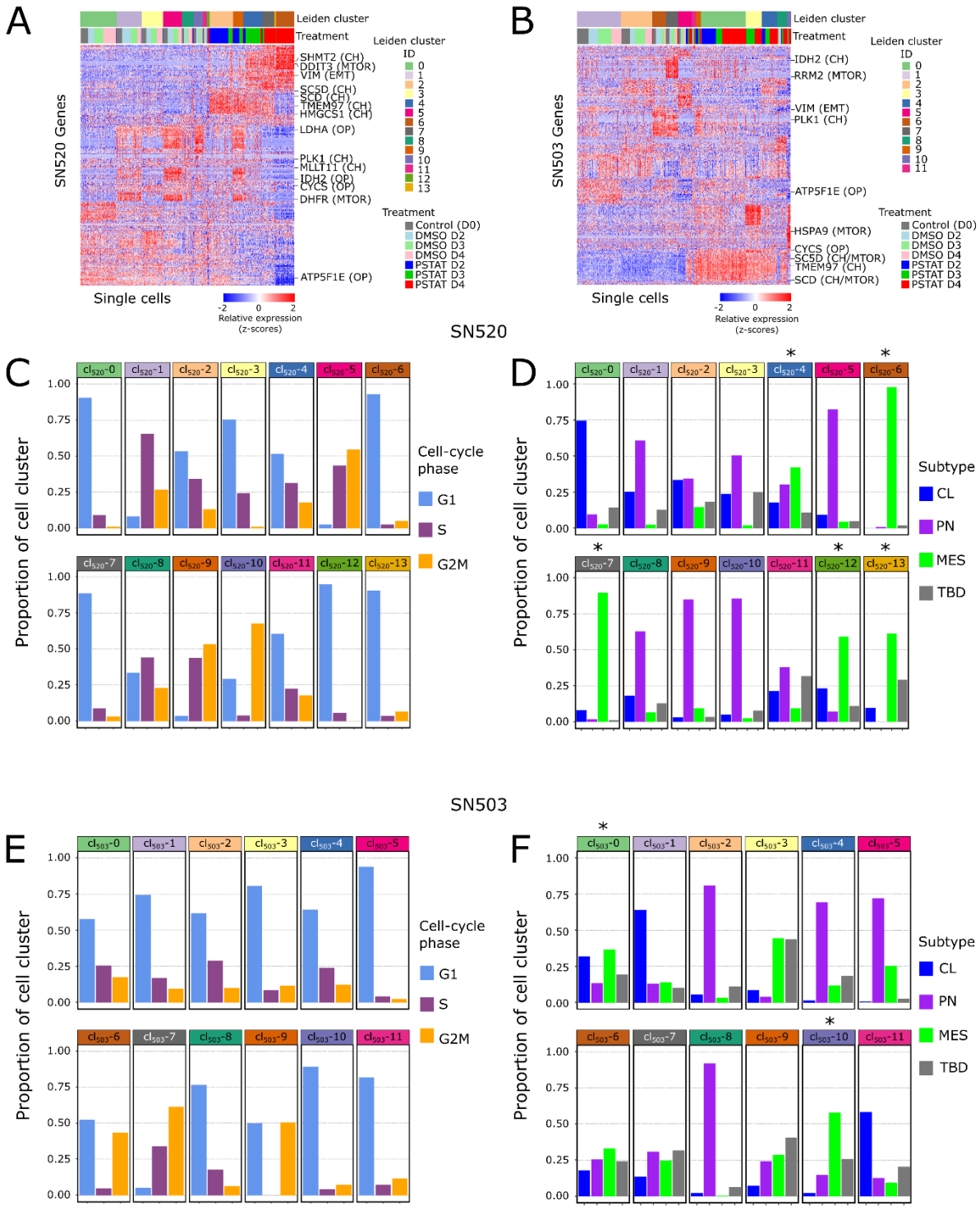

Fig. S8. Leiden cell cluster composition (DEGs, cell cycle phase, and molecular subtypes). (**A**) Heatmap of the top upregulated DEGs, based on FDR values, across the Louvain cell clusters (cl) identified in vehicle-control- and pitavastatin-treated cells for **(A)** SN520 and **(B)** SN503.

Labeled genes are representative members of various enriched hallmark gene sets (CH = cholesterol homeostasis, OP = oxidative phosphorylation, MTOR = MTORC1 signaling, EMT = epithelial-to-mesenchymal transition). Proportions of cells in each cell cycle phase or GBM molecular subtype within each Louvain cluster for SN520 **(C, D)**, and SN503 **(E, F)**, respectively. Asterisks indicate which Louvain cell clusters were enriched for apoptotic gene signatures (Figure 3E).

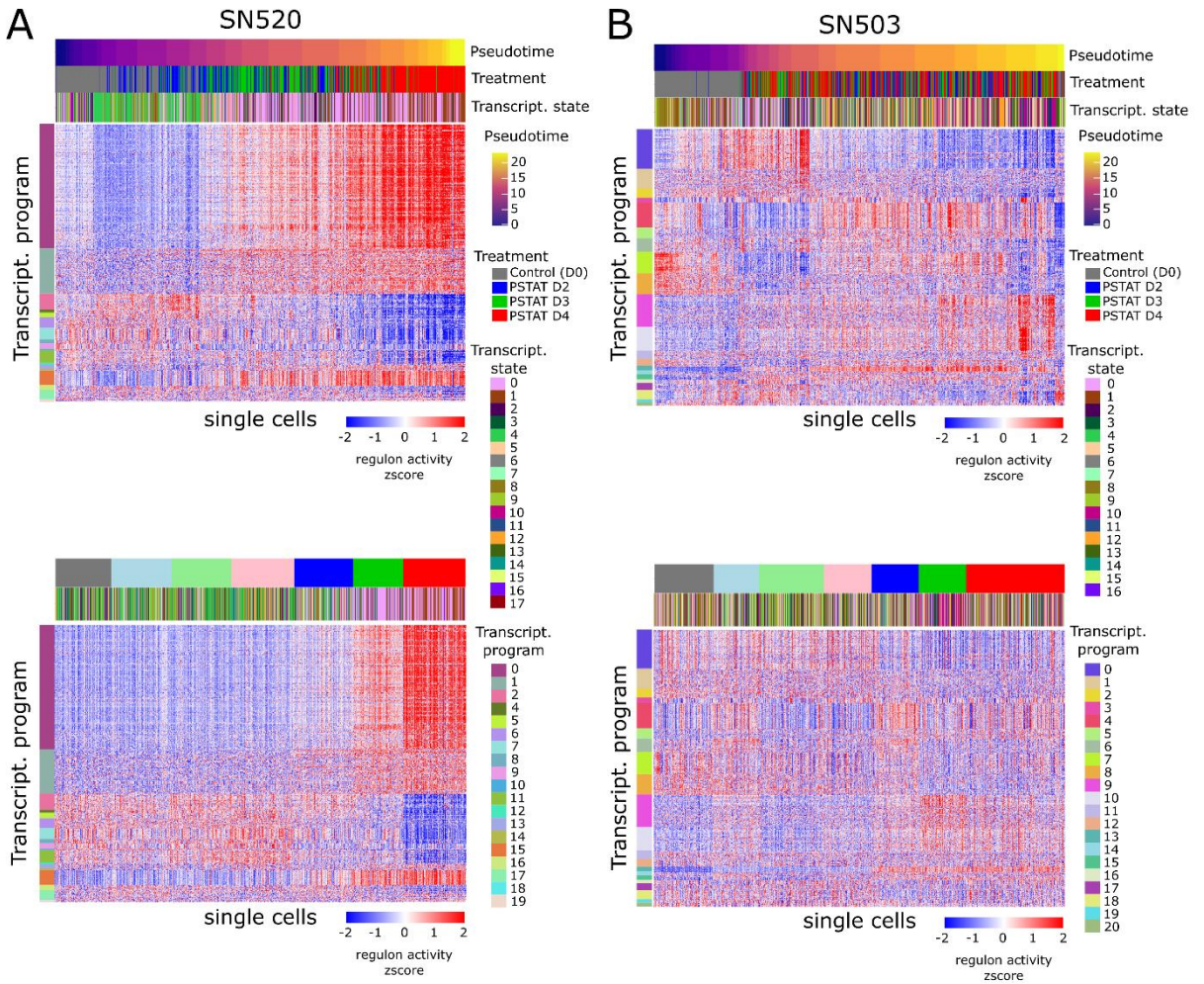

Fig. S9. SN520 and SN503 regulon activities. Heatmaps of eigengene values, i.e., regulon activities and transcriptional programs for **(A)** SN520 and **(B)** SN503. Top row of heatmaps show regulon activities in cells rearranged according to corresponding pseudotime. Bottom row of heatmaps include cells rearranged with respect to experimental treatment. Top color bars represent pseudotime, treatment, and MINER3-inferred transcriptional state.

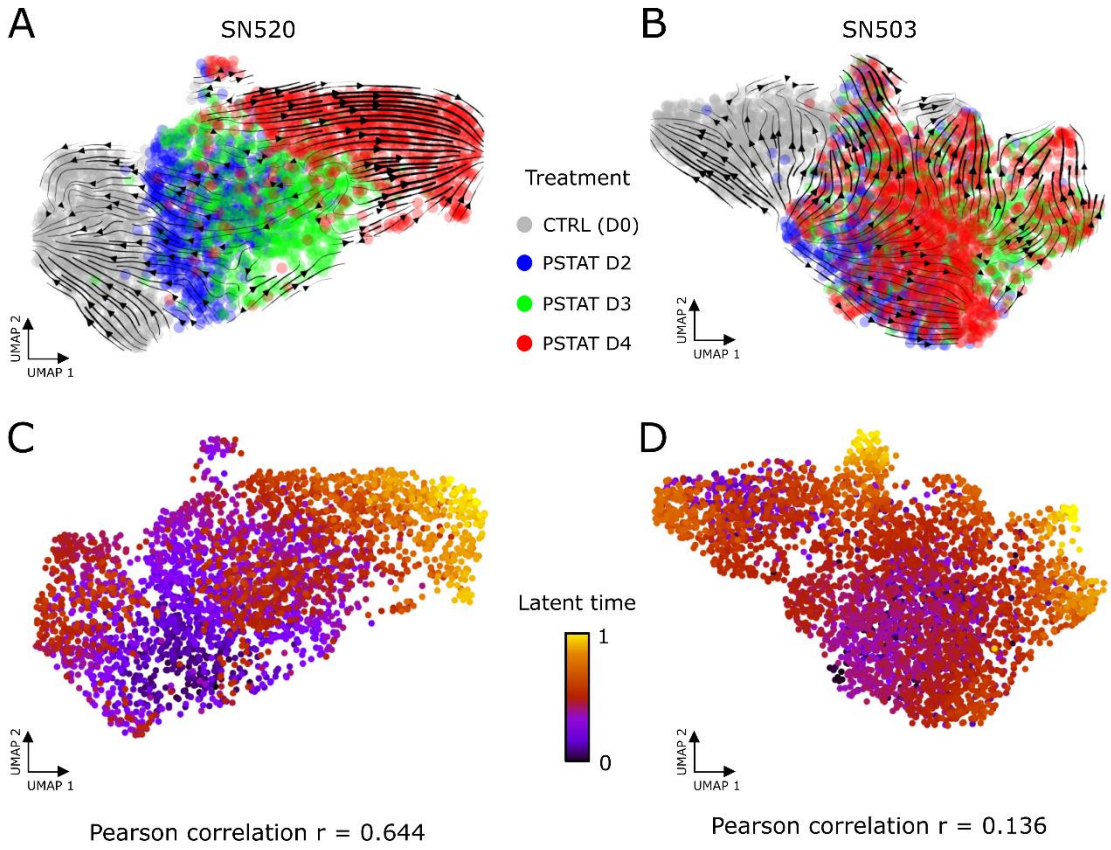

Fig. S10. scVelo analysis. (A – B) RNA velocity and **(C – D)** latent times for SN520 and SN503, respectively. Pearson correlations indicate correlation between latent times and experimental timing across D2 – D4 (control samples excluded).

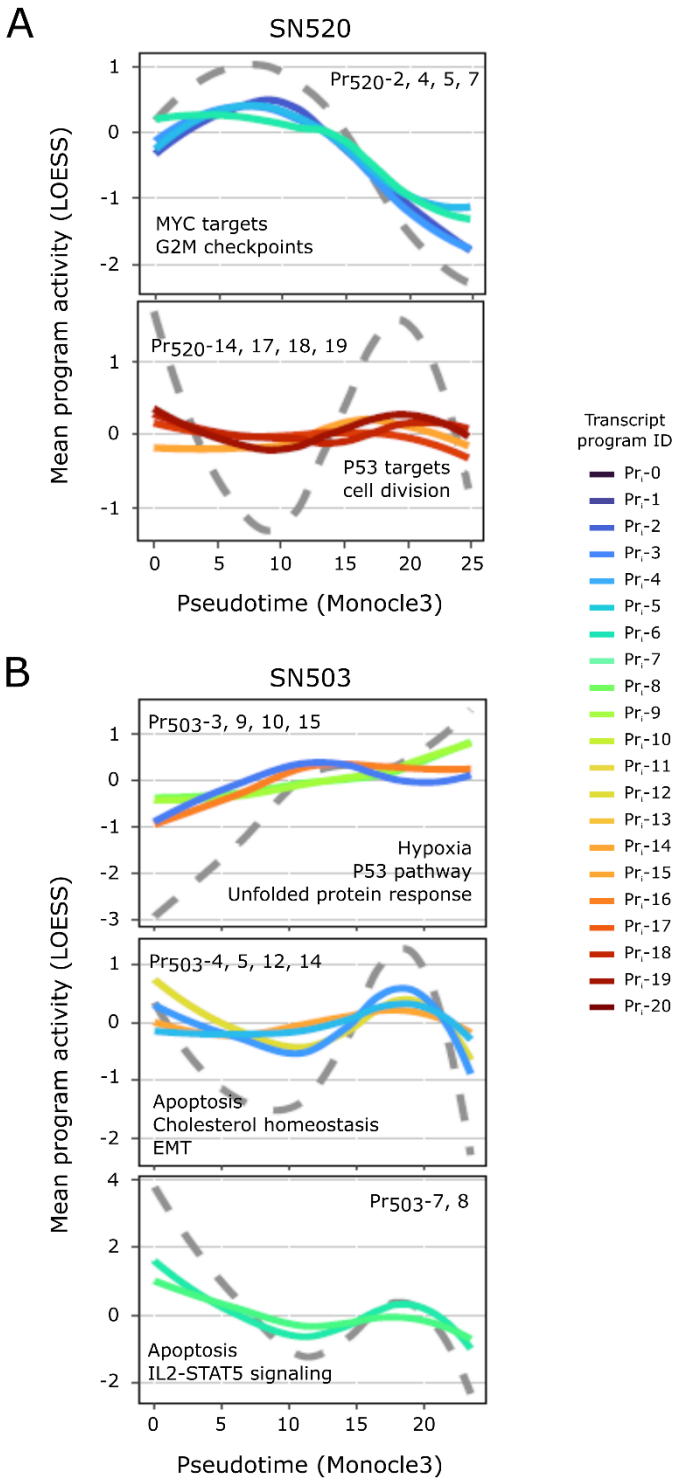

Fig. S11. Transcriptional program activity dynamics. Activity profiles of remaining transcriptional programs not included in main Figure 5D for **(A)** SN520 and **(B)** SN503. Programs were clustered together based on their LOESS regressed activity profiles with respect to

pseudotime. Dashed grey lines represent the average shape of regression profiles for each program cluster. Representative hallmark gene sets enriched within programs are included within each plot.

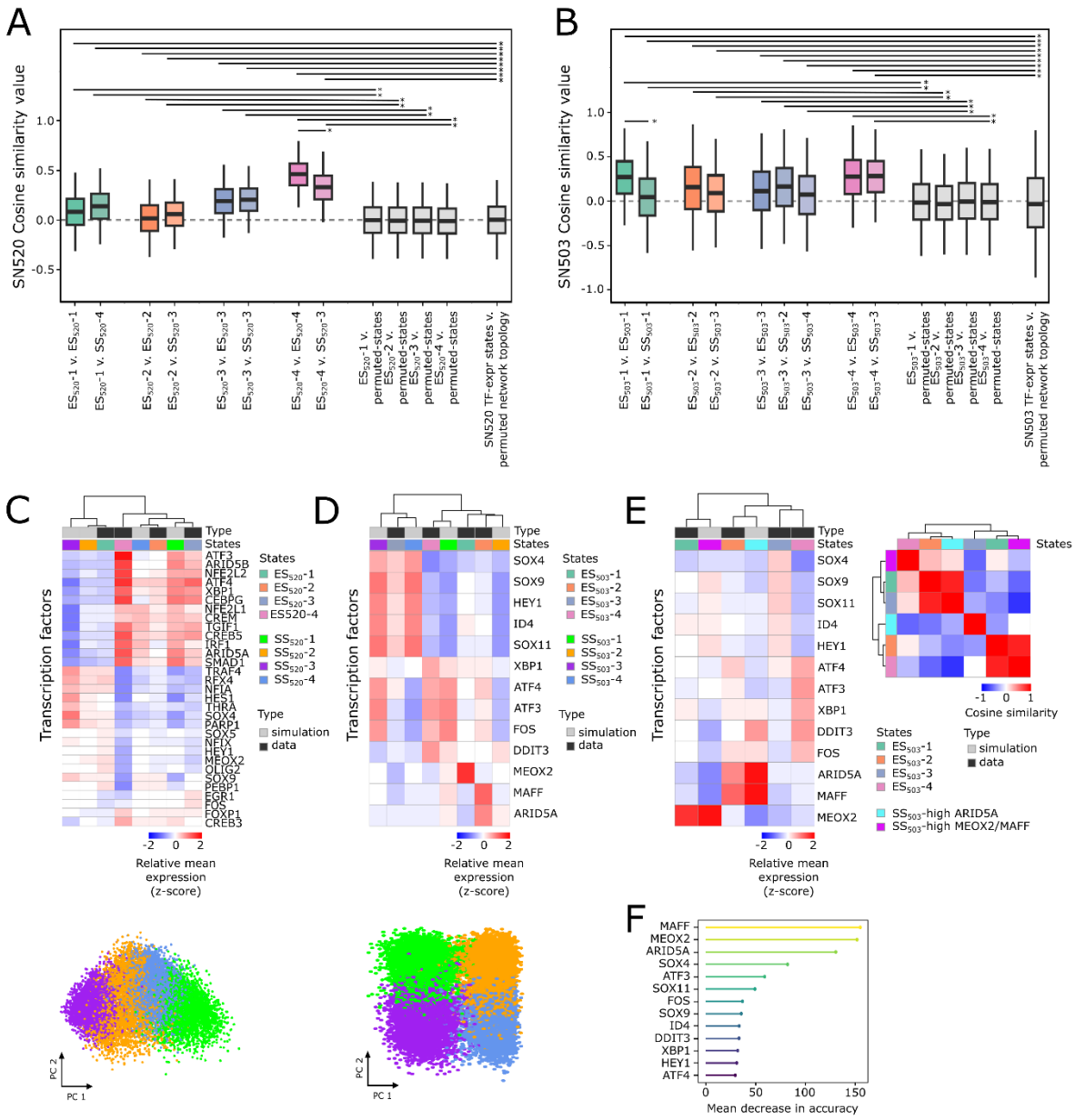

286

287 **Fig. S12. Significance and validation of TF-TF network topologies. (A)** Boxplots of pairwise
288 cosine similarity values based on specific pairwise comparisons of experimental states (ES_{520}-*i*)
289 and simulated states (SS_{520}-*i*) generated from SYGNAL-520. Horizontal lines with adjacent
290 asterisks connecting two distributions indicate that the first (leftmost) distribution is statistically
291 significantly higher (FDR << 0.01). Distribution of cosine similarity values from pairwise
292 comparisons of experimental states (ES_{520}-*i,* colored boxplots) and permutated states (grey
293 boxplots). Permutated states were derived from *i)* permuted expression data, where both cell and
294 gene labels were randomly permuted, and *ii)* randomized network topology (METHODS). **(B)**

Boxplots for SYGNAL-503. Note that multiple simulated states (SS_{503}-2 and SS_{503}-4) showed similarities to ES_{503}-3. **(C)** Heatmap of mean relative expression (z-score) of TFs across cells within each experimental state (ES_{520}) and simulated state (SS_{520}) for SN520, states (columns) are hierarchically clustered. Color bars on top indicate states and data type (grey – simulation or black – experimental data). PCA plot of simulated states from SYGNAL-520 below the heatmap is included for reference. **(D)** Corresponding heatmap of mean relative expression (z-score) of TFs and PCA plot for SN503. **(E)** Heatmap (left) of mean relative expression for TFs in experimental states and subset of simulations from SYGNAL-503 in which the input expression value for ARID5A, MEOX2, and MAFF are high (normalized expression > 1). States (columns) are hierarchically clustered. Color bar above indicates cell states being compared. Adjacent heatmap (right) shows pairwise cosine similarity values of mean relative expression profiles of experimental and simulated states that have high levels of ARID5A, MEOX2, and MAFF. Color bars indicate cell states. **(F)** Dot plot of TFs rank-ordered based on their importance in classifying experimental states for SN503 using random forest analysis.

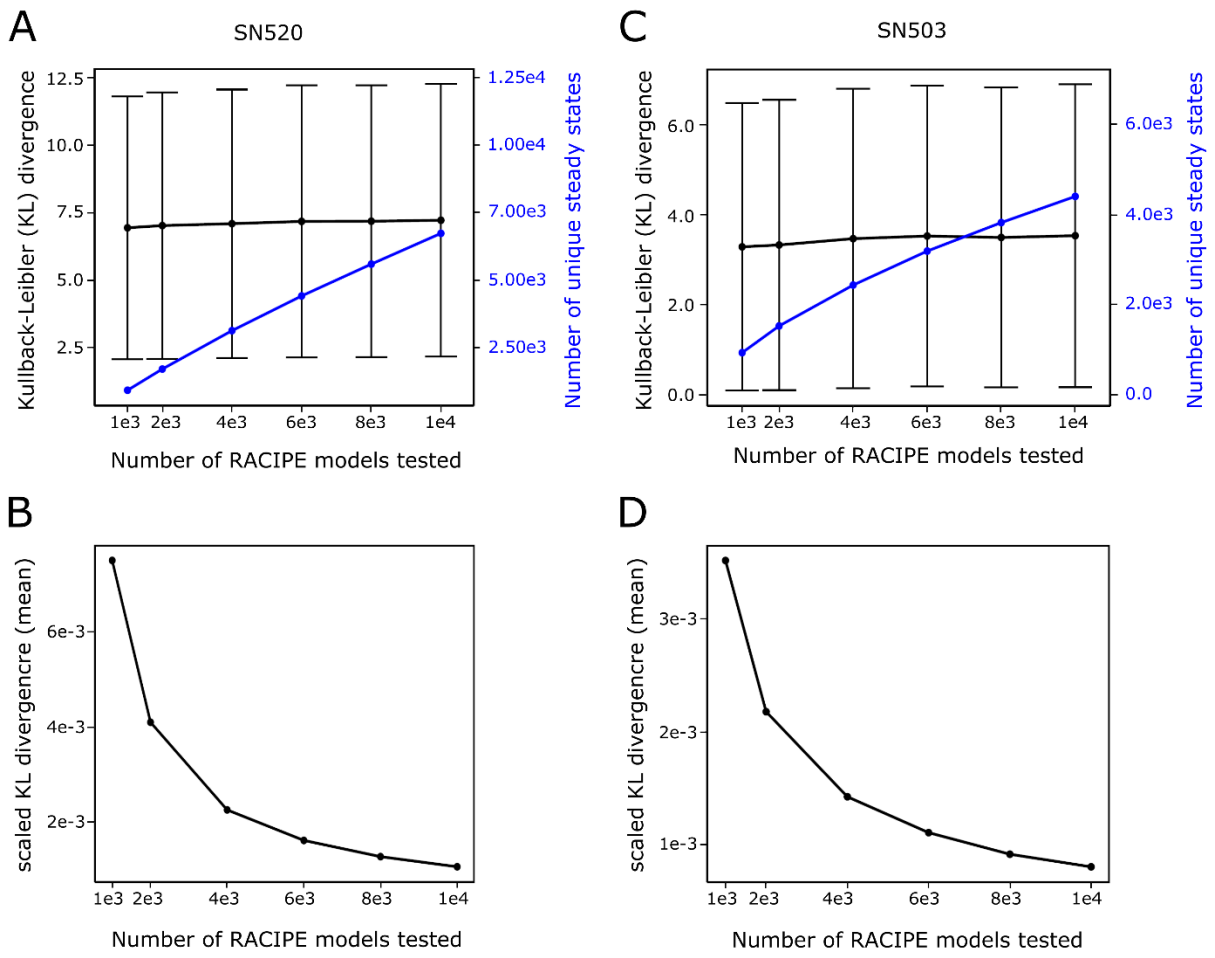

Fig. S13. Convergence of RACIPE simulations of TF-TF networks. (A) Kullback-Leibler divergence distances (black) of simulated states generated by SYGNAL-520 with respect to one another. Simulated states were generated using the respective TF-TF network using a different number of model simulation parameters (1e3, 2e3, 4e3, 6e3, 8e3, and 1e4 randomly selected model parameters) across 100 randomly selected initial conditions. Number of unique states (blue) is based on the number of steady states identified having a specified Euclidean distance greater than its nearest neighbors (METHODS). **(B)** Kullback-Leibler divergence distances normalized with respect to number of unique states identified per set of simulations performed using SYGNAL-520. **(C-D)** Kullback-Leibler divergence distances and normalized distances, respectively, determined from simulations using SYGNAL-503.

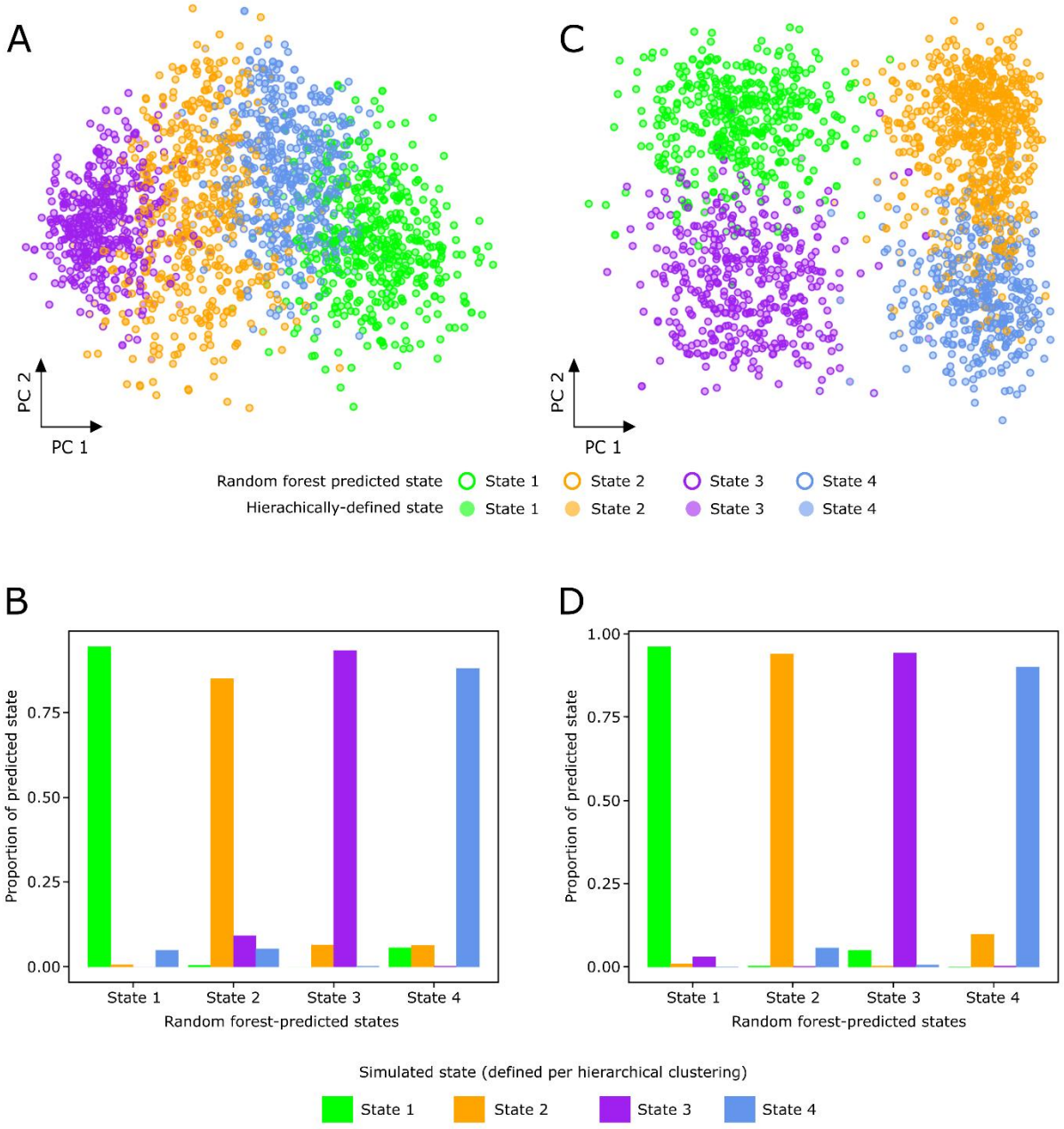

Fig. S14. Random forest model predicts cell state with high-level of accuracy. (A) PCA plot of a randomly selected subset of 2,000 simulated states, i.e., TF expression profile, from the 1e6 simulations performed using SYGNAL-520 (Fig 6C). Each dot represents a simulation output. Fill colors for each dot represent the state of the cell as defined by hierarchical clustering of the cells. Border colors represent the state of the predicted simulated state using the random forest model trained on the non-redundant states generated from the 1e6 simulations (6,519 states and 4,223 states for SN520 and SN503, respectively). **(B)** Proportion of each actual state, defined by

hierarchical clustering, within the predicted simulated states for SN520. **(C)** PCA plot of a randomly selected subset of 2,000 simulated states for SN503. **(D)** Proportion of actual states within each predicted state for SN503.

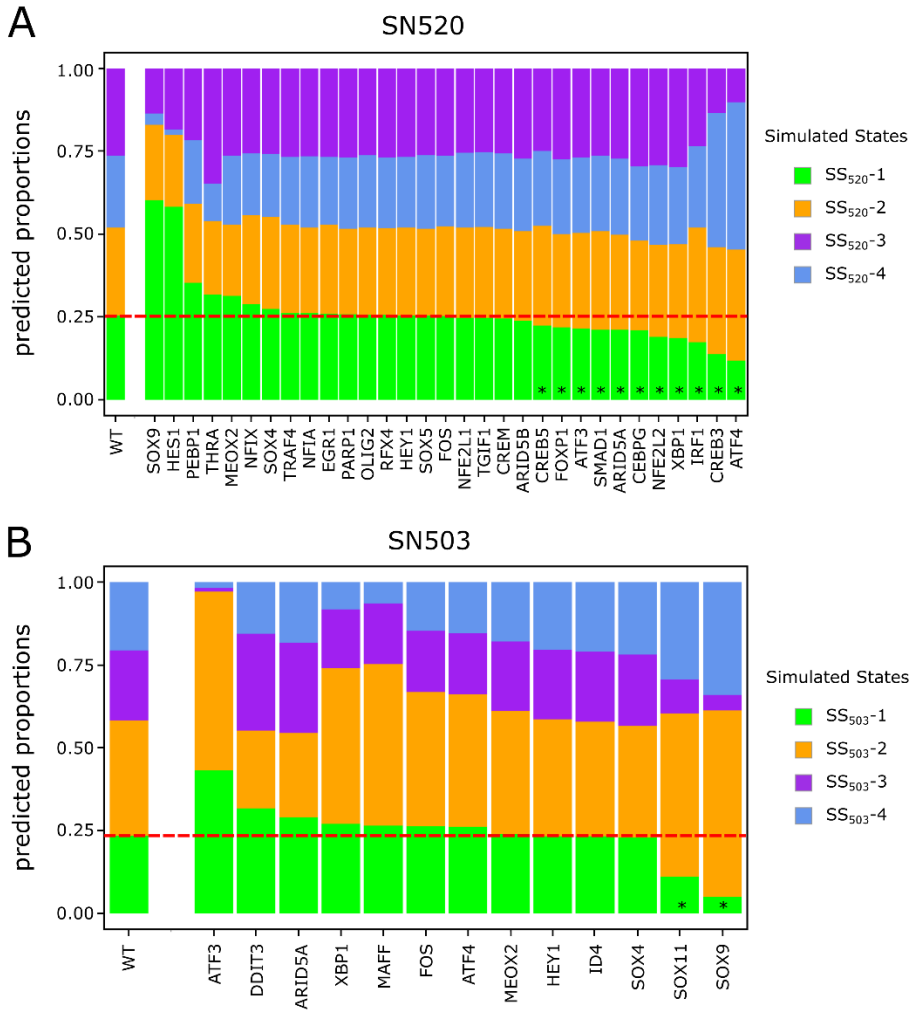

Fig. S15. *In silico* KD simulations in SYGNAL-520/503. (A) Stacked bar plot depicting proportion of simulated states assigned to one of four simulated states (SS_{520}-*i*) identified from hierarchical clustering of RACIPE simulations using SYGNAL-520 (Figure 6C) in response to a 95% knock down (KD) in expression of particular TF. TFs are rank ordered according to the proportion of simulated states assigned to SS_{520}-1 (green), which corresponds to a mesenchymal state. **(B)** Stacked bar plot depicting proportion of simulated states assigned to one of four simulated states (SS_{503}-*i*) identified from hierarchical clustering of RACIPE simulations using SYGNAL-503 (Figure 6E) in response to a 95% knock down (KD) in expression of particular TF. TFs are rank ordered according to the proportion of simulated states assigned to SS_{503}-1, which contained the largest proportion of mesenchymal cells.

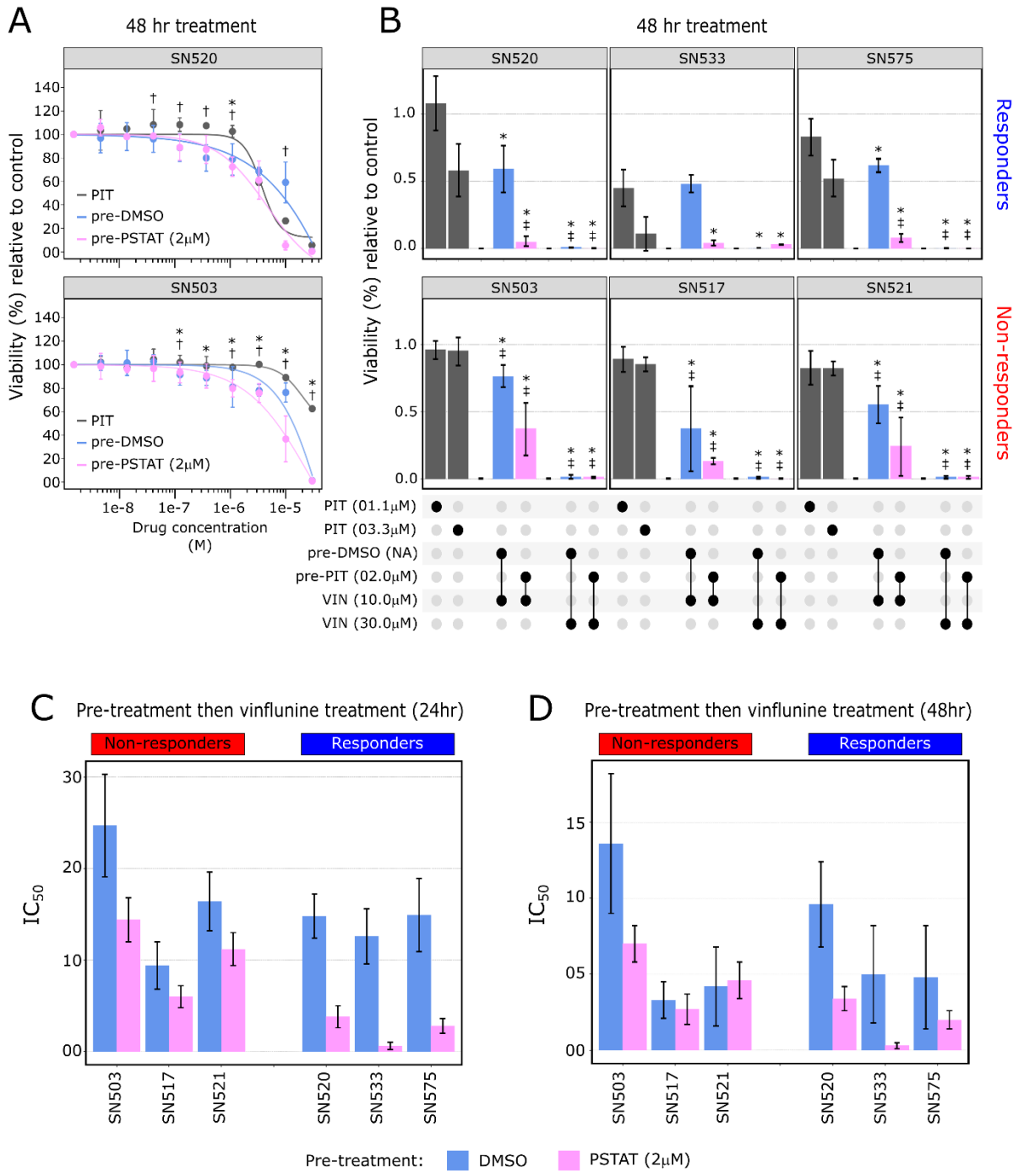

Fig. S16. Pitavastatin pretreatment (48hrs) improves vinflunine efficacy in PD-GSCs. (A) Dose-response curves for SN520 (top) and SN503 (bottom) under pitavastatin monotherapy (at concentrations of 1.5e-9, 4.6e-9, 13.7e-9, 41.2e-9, 123.5e-9, 370.4e-9, 1.10e-6, 3.30e-6, 10.0e-6 30.0e-6 M, dark grey) or combination therapy, which includes pretreatment with DMSO (light blue) or pitavastatin (2μM, pink) for 48hrs and subsequent treatment with vinflunine (at identical

concentrations used in pitavastatin monotherapy). Asterisks indicate cells pretreated with DMSO have significantly lower relative viability than cells treated with pitavastatin alone (FDR $\leq$ 0.1). Crosses indicate cells pretreated with pitavstatin (2μM) have significantly lower relative viabilities than cells treated with pitavastatin alone (FDR $\leq$ 0.1). Error bars represent $\pm$2x standard deviation (N = 3). **(B)** Relative viabilities of PD-GSCs after treatment including monotherapy with pitavastatin (PIT), pretreatment with DMSO (pre-DMSO) or pitavastatin (pre-PIT) followed by vinflunine (VIN) at specified concentrations. Black dots underneath barplots indicate respective treatment(s). Asterisks indicate conditions that have significantly lower relative viability cells treated with pitavastatin alone (1.1μM, FDR $\leq$ 0.1). Double crosses indicate conditions that have significantly lower relative viabilities than cells treated with pitavastatin alone (3.3μM FDR $\leq$ 0.1). Colors correspond to annotation in (A). Error bars represent $\pm$2x standard deviation (N=3). (C) IC50 values based on 72hr pre-treatment with either DMSO or pitavastatin (2μM) followed by 24hr treatment with vinflunine. (D) IC50 values based on 72hr pre-treatment with either DMSO or pitavastatin (2μM) followed by 48hr treatment with vinflunine. Error bars in (C-D) represent $\pm$2x standard deviation (N = 3).

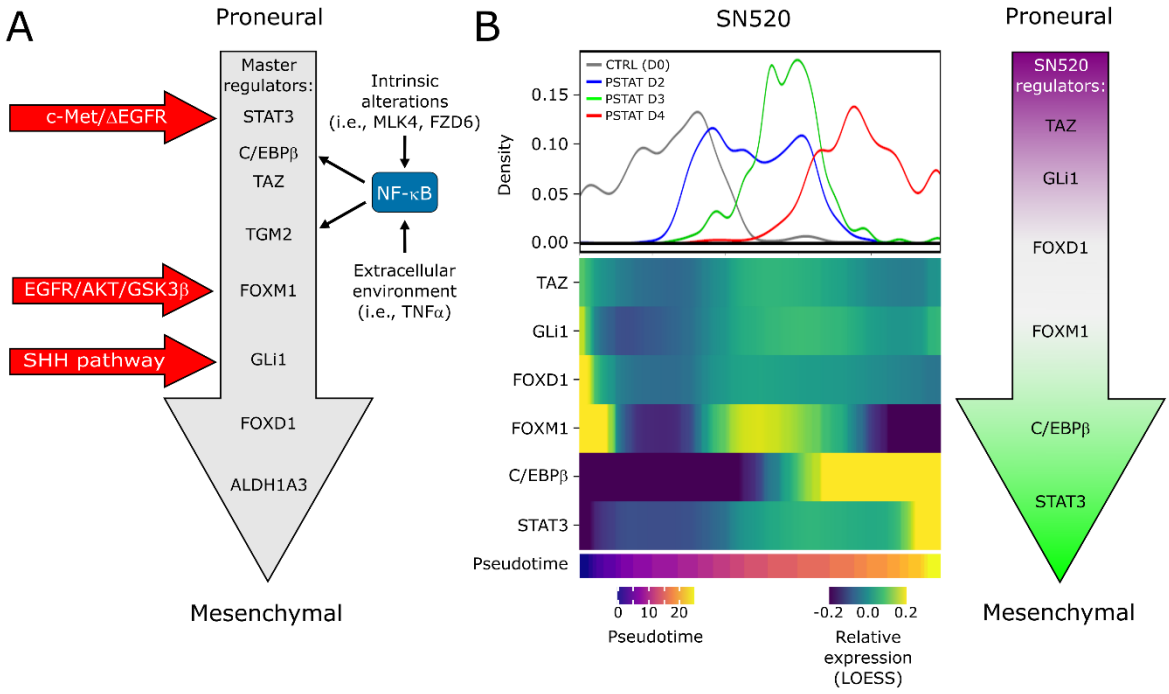

Fig. S17. SN520 exhibits a sequence of TF expression distinct from previously proposed mechanisms of PMT. (A) Master regulators driving PMT in GBM. Figure modified from *(58)*. **(B)** Sequence of TF expression of master regulators per *(58)* observed in SN520. Density plot and heatmap align with pseudotime (bottom color bar). Density plot shows proportion of cells belonging to each treatment condition arranged according to pseudotime. Heatmap shows relative expression (LOESS regression) of TF expression along pseudotime. TFs listed are master regulators overlapping in SN520 scRNA-seq data set. TFs are listed in sequential order according to their peak expression, which differs considerably from (A).

Table S1 – S16 (separate file)

Supplementary tables referenced in manuscript.

Table S1.

Enriched gene sets in up-regulated DEGs in each treatment condition - SN520.

Table S2.

Enriched gene sets in up-regulated DEGs in Louvain clusters - SN520.

Table S3.

Enriched gene sets in up-regulated DEGs in each treatment condition - SN503.

Table S4.

Enriched gene sets in up-regulated DEGs in Louvain clusters - SN503.

Table S5.

SN520 regulon summary.

Table S6.

SN520 miRNA regulators (FIRM results).

Table S7.

Enrichment of essential GSC genes (MacLeod et al. 2019) in SN520 transcriptional programs.

Table S8.

SN520 gene set enrichment of transcriptional programs.

Table S9.

SN503 regulon summary.

Table S10.

SN503 miRNA regulators (FIRM results).

Table S11.

Enrichment of essential GSC genes (MacLeod et al. 2019) in SN503 transcriptional programs.

Table S12.

SN503 gene set enrichment of transcriptional programs.

Table S13.

Transcription factor summary of TF-TF networks.

Table S14.

PD-GSC metadata.

Table S15.

HDAC-inhibition DEG overlap count and enrichment in PD-GSC DEGs.

Table S16.

Experimental inoculation densities.